MATERIALS CHEMISTRY FRONTIERS

RESEARCH ARTICLE

View Article Online
View Journal | View Issue

Cite this: *Mater. Chem. Front.*, 2022, **6**, 2085

A large-scale deep-blue tetraphenylbenzene-bridged hybridized local and charge transfer fluorophore exhibiting small efficiency roll-off and low amplified spontaneous emission threshold†

Shian Ying,[ab] Jichen Lv,[a] Yuanzhao Li,[b] Yumiao Huo,[c] Yuchao Liu,[a] Dongge Ma,[b] Ling Peng*[a] and Shouke Yan*[ad]

Efficient and stable deep-blue organic luminescent materials are important but rare for application in full-color displays due to their intrinsic wide bandgap characteristics. Here, a high-performance deep-blue hybridized local and charge transfer fluorophore **PTPC** with the aggregation enhanced emission (AEE) effect has been designed and synthesized with 1,2,4,5-tetraphenylbenzene as the bridge. High morphological stability, high photoluminescence efficiency, fast radiative rate, suitable energy levels, and bipolar-transporting properties are obtained simultaneously by incorporating a twisted molecular skeleton with weak, rigid and nearly flat donor/acceptor groups. As a result, a high forward-viewing external quantum efficiency of 6.78% as well as a deep-blue emission with the Commission Internationale de l'Eclairage coordinates of (0.156, 0.059) is achieved in a non-doped organic light-emitting diode (OLED). The EQEs still remain as high as 6.73% and 6.18% at 100 and 1000 cd m^{-2}, showing a small efficiency roll-off. Furthermore, **PTPC** exhibits extraordinary amplified spontaneous emissions (ASEs) with a low threshold of 1.18 μJ cm^{-2} and a gain coefficient of 36.6 cm^{-1}. This work provides a new insight into creating high-performance deep-blue organic semiconductors with marked ASE performance for further practical applications.

Received 29th May 2022,
Accepted 22nd June 2022

DOI: 10.1039/d2qm00506a

rsc.li/frontiers-materials

Introduction

With the rapid development of high and ultrahigh definition displays, highly efficient and stable blue organic optoelectronic materials have been a major requirement for applications in organic light-emitting diodes (OLEDs) and organic solid-state lasers (OSSLs).[1–5] However, although extensive efforts have been devoted, owing to the intrinsic wide bandgap characteristics, high-performance and cost-effective deep-blue emitters and devices meeting the requirement of Commission Internationale de l'Eclairage (CIE) y coordinate value <0.06 are really rare.[6] So far, blue phosphorescent and thermally activated delayed fluorescence (TADF) OLEDs have realized high external quantum efficiencies (EQEs) exceeding 25%,[7–11] but the emitters have to be dispersed into an appropriate host matrix to alleviate the concentration quenching effect,[12–14] which not only requires a stable host and adjacent layers with high triplet state energy (E_T) higher than that of the emitters, but is also related to host–guest doping technology, posing the phase separation risk and increasing the production costs.[13,15] In addition, the phosphorescent and TADF OLEDs usually suffer from serious efficiency roll-off at high current density, resulting from exciton annihilation involving long-lived triplet excitons.[16,17] Despite the ease of achieving deep-blue emitters based on triplet–triplet annihilation (TTA) and hybridized local and charge transfer (HLCT) mechanisms, achieving high efficiency OLEDs needs very delicate molecular and device engineering.[18–22] Thus, continued effort is still urgent to pursue stable and efficient deep-blue pure organic light-emitting materials and non-doped OLEDs with CIEy $<$ 0.06 for application in (ultra-) high definition displays.

[a] *Key Laboratory of Rubber-Plastics, Ministry of Education, Qingdao University of Science and Technology, Qingdao 266042, P. R. China. E-mail: pengling615@163.com, skyan@mail.buct.edu.cn*
[b] *Institute of Polymer Optoelectronic Materials and Devices, State Key Laboratory of Luminescent Materials and Devices, South China University of Technology, Guangzhou 510640, P. R. China*
[c] *College of Materials Science and Engineering, Shandong University of Science and Technology, Qingdao 266590, P. R. China*
[d] *State Key Laboratory of Chemical Resource Engineering, College of Materials Science and Engineering, Beijing University of Chemical Technology, Beijing 100029, P. R. China*

† Electronic supplementary information (ESI) available. See DOI: https://doi.org/10.1039/d2qm00506a

Designing an excellent deep-blue emitter should indeed meet several criteria with regard to color quality, efficiencies, stability, and charge-carrier injection/transportation:[3,4,23–25] (1) satisfying the standard of CIEy < 0.06 with good emission color purity, which is essential to develop high-end electronic displays such as (ultra-) high definition televisions, (2) a high photoluminescence quantum yield (PLQY), generally, the higher the PLQY is, the better the electroluminescence (EL) performance of the device will be achieved, (3) high thermal and morphological stabilities, which is beneficial for extending the lifetime of OLEDs, and (4) suitable highest occupied molecular orbital (HOMO) and lowest unoccupied molecular orbital (LUMO) energy levels, which can ensure efficient hole and electron injection, transportation, and recombination within the emissive layer. To achieve deep-blue emission, the π-conjugation length of molecules must be limited, which in turn imposes restraint on the molecular size. Nevertheless, the limited molecular size is detrimental to forming morphologically stable and uniform amorphous films.[4] On the other hand, deep-blue materials should have a high PLQY to realize a high EQE in the device. The PLQY at the aggregation-state can be enhanced by impeding intermolecular π–π packing interactions, and increasing the conjugated degree of the emitter that is dependent on the molecular rigidity and planarity. However, the enlargement of molecular planarity will lead to strong π–π packing and bathochromic shift of emission. Therefore, achieving a good trade-off among the necessary properties to develop high-performance deep-blue emitters and non-doped devices really represents a challenging scientific task to researchers.

1,2,4,5-Tetraphenylbenzene (1,2,4,5-TPB) featuring the typical aggregation enhanced emission (AEE) characteristic possesses moderate dihedral angles of 40.50–65.98°.[26] The rigid and twisted molecular structure makes it realize an efficient ultraviolet emission peak at ∼363 nm in the aggregate state due to restriction of intramolecular motion. These properties are beneficial to construct pure blue emitters by linking appropriate electron-donating and accepting groups.[27–29] However, It is difficult to build high-performance non-doped deep-blue OLEDs with CIEy < 0.06 and EQE ≥ 5%.[30] What's more, the efficiency roll-off at high luminance needs to be improved in the 1,2,4,5-TPB-based OLEDs. In this study, we designed and synthesized a large-scale donor–π–acceptor (D–π–A) type HLCT material **PTPC** with 1,2,4,5-TPB as the π-bridge linking weak, rigid, and bulky donor (D) and acceptor (A) units. This not only interrupts the π-conjugation and relieves the intramolecular charge transfer between D and A units by the 1,2,4,5-TPB spacer, realizing a deep-blue emission, but also increases the length and rigidity of the non-coplanar molecular skeleton and suppresses the rotation or vibration of groups, achieving a high PLQY and radiative rate in the pure film state. As a result, the non-doped device with the compound **PTPC** as the emitter realizes deep-blue light with the EL peak at 411 nm and a narrow full width at half maximum (FWHM) of 55 nm, corresponding to the CIE coordinates of (0.158, 0.059). It is worthwhile to note that a high forward-viewing EQE of 6.78% is achieved and the value remains as high as 6.18% at a practical brightness of 1000 cd m^{-2}. Encouragingly, owing to the high PLQY and fast radiative rate ($S_1 \rightarrow S_0$ transition) exceeding 8×10^8 s^{-1}, **PTPC** exhibits excellent amplified spontaneous emission (ASE) characteristics with a low threshold of 1.18 μJ cm^{-2}.

Experimental methods

Synthesis and characterization of materials

Synthesis of 2′,5′-dibromo-1,1′:4′,1″-terphenyl (TP-Br). Under an N_2 atmosphere, 1,4-dibromo-2,5-diiodobenzene (4.88 g, 10 mmol), phenylboronic acid (2.74 g, 22.5 mmol), and tetrakis(triphenylphosphine)palladium(0) (0.41 g, 0.35 mmol) were dissolved in 50 mL of toluene. And 2 M potassium carbonate (6.91 g, 50 mmol) in 25 mL of water and CH_3CH_2OH (25 mL) were added to the reaction mixture. Then the reaction mixture was stirred at 95 °C for 20 hours. After cooling to ambient temperature, the reaction mixture was extracted with dichloromethane and water and dried by anhydrous magnesium sulfate. The organic layer after filtration was evaporated under reduced pressure with a rotary evaporator. The crude product was further purified by silica-gel column chromatography using petroleum as the solvent and finally dried under vacuum to give a white solid (2.94 g, yield: 70%). ^{1}H NMR (400 MHz, $CDCl_3$, δ, ppm): 7.66 (s, 2H), 7.50–7.39 (m, 10H).

Synthesis of 9-(4′-bromo-[1,1′-biphenyl]-4-yl)-3,6-di-*tert*-butyl-9*H*-carbazole (tCZ-Br). 3,6-Bis(*tert*-butyl)-9*H*-carbazole (2.79 g, 10 mmol), 4-bromo-4′-iodobiphenyl (3.95, 11 mmol), copper(I) iodide (1.90 g, 10 mmol) and potassium carbonate (2.76 g, 20 mmol) were dissolved in 50 mL of *N*,*N*-dimethylformamide in a 250 mL 2-neck round bottom flask under a nitrogen atmosphere. The reaction mixture was refluxed for 12 hours with continuous stirring. Then the solvent was removed under reduced pressure. The reaction mixture was extracted with dichloromethane and water and dried using anhydrous magnesium sulfate. After filtration and evaporation under reduced pressure with a rotary evaporator, the crude product was further purified by silica-gel column chromatography using dichloromethane/petroleum (1/5, v/v) as the solvent and finally dried under vacuum to give a white solid (4.17 g, yield: 75%). ^{1}H NMR (400 MHz, $CDCl_3$, δ, ppm): 8.18 (s, 2H), 7.76 (d, J = 8.4 Hz, 2H), 7.67–7.60 (m, 4H), 7.58–7.52 (m, 2H), 7.49 (d, J = 9.3 Hz, 2H), 7.42 (d, J = 8.6 Hz, 2H), 1.50 (s, 18H).

Synthesis of 3,6-di-*tert*-butyl-9-(4′-(4,4,5,5-tetramethyl-1,3,2-dioxaborolan-2-yl)-[1,1′-biphenyl]-4-yl)-9*H*-carbazole (tCZ-B). Under an N_2 atmosphere, tCZ-Br (2.55 g, 5 mmol), bis(pinacolato) diboron (1.91 g, 7.5 mmol), [1,1′-bis(diphenylphosphino) ferrocene]dichloropalladium(II) Pd(dppf)Cl_2 (0.15 g, 0.2 mmol), KOAc (1.47 g, 15 mmol) and 50 mL of 1,4 dioxane were added into a 250 mL 2-neck round-bottom flask and heated at 110 °C for 15 hours. Then the reaction mixture was cooled down to room temperature, extracted with dichloromethane, and dried over anhydrous magnesium sulfate. The organic layer was filtered and purified by silica-gel column chromatography with dichloromethane/petroleum (1/3, v/v) as the solvent. Finally, the product was further dried under vacuum to give a white solid (3.83 g, yield: 90%).^{1}H NMR

(500 MHz, $CDCl_3$, δ, ppm): 8.16 (s, 2H), 7.96 (d, J = 7.8 Hz, 2H), 7.83 (d, J = 7.6 Hz, 2H), 7.72 (d, J = 7.7 Hz, 2H), 7.64 (d, J = 8.2 Hz, 2H), 7.48 (d, J = 8.7 Hz, 2H), 7.42 (d, J = 8.6 Hz, 2H), 1.49 (s, 18H), 1.40 (s, 12H).

Synthesis of 9-(5′-bromo-4′-phenyl-[1,1′:2′,1″:4″,1‴-quaterphenyl]-4‴-yl)-3,6-di-*tert*-butyl-9*H*-carbazole (TPC-Br). The procedure was analogous to that described for TP-Br. As a result, the crude product was purified by silica-gel column chromatography using dichloromethane/petroleum (1/5, v/v) as the solvent and finally dried under vacuum to give a white solid (yield: 72%). ^{1}H NMR (500 MHz, $CDCl_3$, δ, ppm): 8.19 (s, 2H), 7.82 (s, 1H), 7.79 (d, J = 8.1 Hz, 2H), 7.62 (d, J = 7.5 Hz, 2H), 7.57 (s, 4H), 7.52 (s, 5H), 7.45 (d, J = 7.2 Hz, 1H), 7.41 (d, J = 8.6 Hz, 2H), 7.33–7.26 (m, 7H), 1.50 (s, 18H).

Synthesis of 2-(4‴-(3,6-di-*tert*-butyl-9*H*-carbazol-9-yl)-2′,5′-diphenyl-[1,1′:4′,1″:4″,1‴-quaterphenyl]-4-yl)-1-phenyl-1*H*-phenanthro[9,10-*d*]imidazole (PTPC). The procedure was analogous to that described for TP-Br. As a result, the crude product was purified by silica-gel column chromatography using dichloromethane/petroleum (2/1, v/v) as the solvent and finally dried under vacuum. Then the resulting compound was further purified by recrystallization with the mixed solvent ethanol and toluene to give a white solid (yield: 68%). ^{1}H NMR (500 MHz, $CDCl_3$, δ, ppm): ^{1}H NMR (500 MHz, $CDCl_3$, δ, ppm): 8.91 (s, 1H), 8.78 (d, J = 8.4 Hz, 1H), 8.72 (d, J = 8.4 Hz, 1H), 8.18 (s, 2H), 7.80 (d, J = 8.3 Hz, 2H), 7.76 (d, J = 7.6 Hz, 1H), 7.67 (t, J = 7.7 Hz, 1H), 7.65–7.45 (m, 17H), 7.41 (d, J = 8.6 Hz, 2H), 7.37 (d, J = 8.2 Hz, 2H), 7.33–7.26 (m, 10H), 7.23–7.18 (m, 3H), 1.50 (s, 18H).^{13}C NMR (125 MHz, $CDCl_3$, δ, ppm): 150.69, 142.88, 141.43, 140.85, 140.63, 140.10, 139.76, 139.34, 139.17, 139.08, 138.94, 138.67, 138.42, 137.34, 132.99, 130.43, 130.09, 129.90, 129.87, 129.73, 129.26, 129.07, 128.26, 128.13, 127.29, 127.11, 126.88, 126.79, 126.56, 126.25, 125.64, 124.89, 124.10, 123.61, 123.40, 123.10, 122.97, 120.84, 116.23, 109.23, 34.72, 32.01. TOF-MS (ESI) m/z calcd for C77H61N3: 1028.3283; $[M + H]^+$ found: 1028.4933.

Results and discussion

Molecular design strategy and synthesis

Donor–acceptor (D–A) type molecules consisting of electron-rich and electron-deficient moieties have been considered as an effective way to develop high-performance emitters due to their bipolar-transporting characteristics. However, these molecules generally create a strong intramolecular charge-transfer state, inducing a large red-shift of emission and a broad FWHM. To circumvent such a problem, on the one hand, rigid and bulky group phenanthrimidazole (PI) with good thermal stability was selected as the weak A unit, while rigid-flexible group 9-phenyl-3,6-di-terbutyl-carbazole (tPCz) possessing a similar HOMO energy level with the PI group was used as the D unit (Fig. S1, ESI†). The introduction of *tert*-butyl at the 3,6-position of carbazole can not only suppress the generation of radical cations or/and anions upon electrochemical oxidation or/and reduction, stabilizing electrical operation of the device, but also decrease the intermolecular π–π interactions and improve the solubility of compound. On the other hand, introducing 1,2,4,5-TPB as the π-bridge linking D and A unit at *para*-positions can interrupt the π-conjugation of both donor and acceptor units. As a result, the rigid and twisted D–π–A type deep-blue emitter **PTPC** with a large non-coplanar molecular skeleton was successfully designed.

As illustrated in Scheme 1, the intermediate **tCZ-Br** was synthesized by the Ullmann reaction, while **tCZ-Br** was obtained by the Miyaura borylation reaction. The target compound **PTPC** was synthesized *via* three-step Suzuki cross-coupling reactions with tetrakis(triphenylphosphine)palladium as the catalyst. The chemical structures of the target compound were determined by the ^{1}H and ^{13}C NMR spectroscopies, and high-resolution mass spectrometry. The detailed synthetic procedures and characterization data were described in the Experimental methods.

Thermal properties and morphological stability

The thermal properties of **PTPC** were examined by using TGA and DSC measurements. As shown in Fig. S1a (ESI†), the

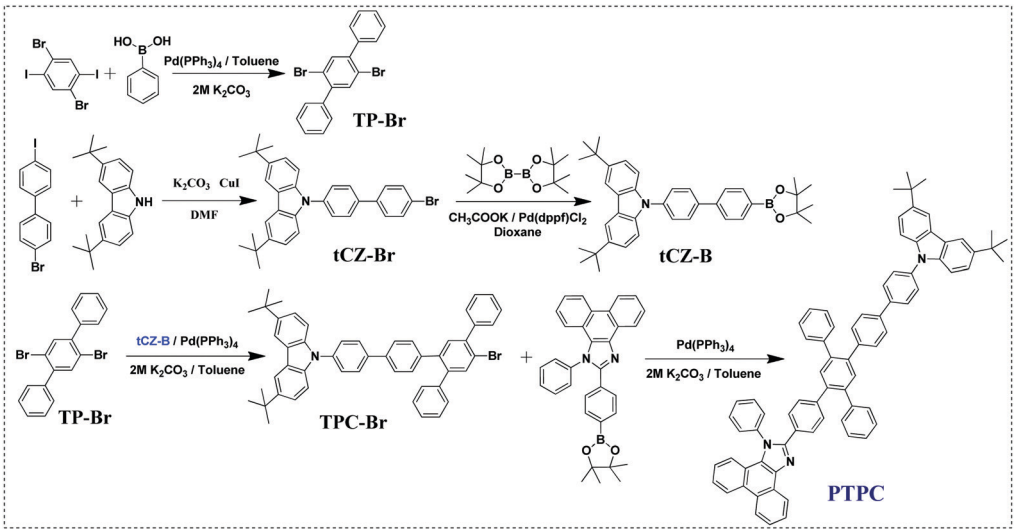

Scheme 1 Synthesis routes and molecular structures of intermediates and **PTPC**.

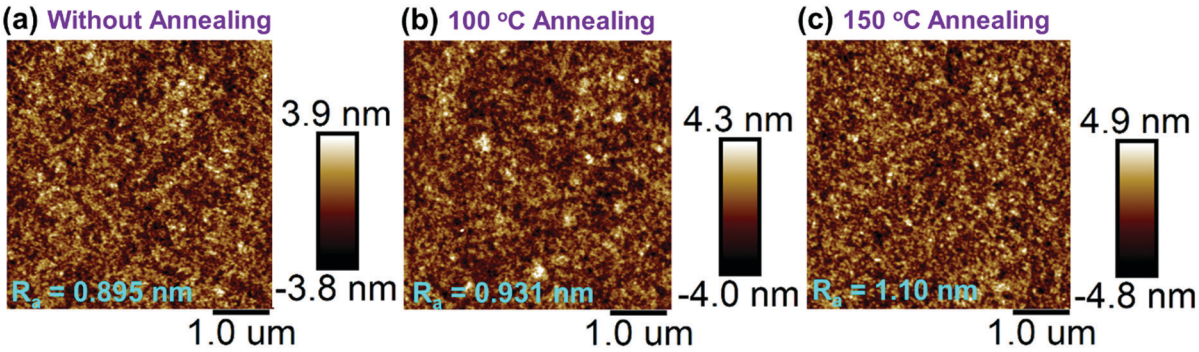

Fig. 1 AFM images of vacuum-evaporation films without annealing (a), and with annealing under 100 (b) and 150 °C (c) for 24 hours in air.

decomposition temperature (T_d) corresponding to 5% weight loss appeared at 520 °C, whereas the glass-transition temperature (T_g) was not detected in the temperature range from 20 to 300 °C, illustrating that the compound could form amorphous films in the wide temperature range. To verify this, we further investigated the morphological stability of 40 nm-thick vacuum-evaporation films of **PTPC** by annealing at different temperatures in the atmosphere. As displayed in Fig. 1 and Fig. S2b, c (ESI†), compared with the film without annealing, after annealing at 100 and 150 °C for 24 hours, the films not only show slight variations in the average surface roughness (R_a) values performed by atomic force microscopy (AFM), but also exhibit stable and unchanged emission spectra. This result proves that high-quality films with good morphological stability can be achieved based on the compound **PTPC**, which is conducive to the development of long-lived OLEDs.

Theoretical calculations

As shown in Fig. 2, geometry optimization in the ground state and FMO calculations were carried out *via* the DFT method at the RB3LYP/6-31G(d,p) level. The LUMO of the compound **PTPC** is mostly delocalized on 1,2,4,5-TPB and extended to the adjacent phenyl ring and several segments in the PI unit, while the HOMO is mainly localized on the tPCz unit with a residual on the PI unit, and the HOMO−1 is mainly distributed on the PI unit the adjacent phenyl ring with a residual on the tPCz unit. This type of orbital feature containing spatial separation in conjunction with a certain degree of overlap is of benefit to the improvement of fluorescence intensity. Moreover, **PTPC** shows a large and highly twisted molecular skeleton with torsion angles of ∼48°–51° between the central phenyl group and external phenyl ring in the 1,2,4,5-TPB core, torsion angles of 27.26°/37.41° between 1,2,4,5-TPB and the PI/tPCz unit, and a large torsion angle of 53.27° between the phenyl ring and carbazole in the tPCz unit, respectively. The efficacious integration between the twisted molecular geometry and rigid and bulky chromophores limits the π-conjugation length, weakens the intramolecular charge transfer intensity, and overcomes the intermolecular stacking interactions in the solid-state, which can prevent aggregation-caused fluorescence quenching, and further achieve more efficient luminescence of the emitter for OLEDs. To further explore the nature of the excited state, NTO analyses were also performed (Fig. S3 and Table S1, ESI†). For the $S_0 \rightarrow S_1$ transition of **PTPC**, the hole is mostly distributed on the whole molecular backbone, while the particle is localized on 1,2,4,5-TPB and extended to the adjacent phenyl and imidazole rings, which clearly reflects the formation of the HLCT excited state. It should be noted that the $S_0 \rightarrow S_1$ excitations can mainly be attributed to the combination of HOMO and HOMO−1 to LUMO transitions (70% and 20%), which ensures the efficient overlap between hole and particle distributions, being beneficial for enhancing the PLQY, corresponding to a large oscillator strength of 1.3043. However, for the $S_0 \rightarrow T_1$ excitations, both holes and particles are mainly delocalized to phenanthrene and adjacent imidazole and biphenyl rings groups, showing an obvious locally excited (LE) state.

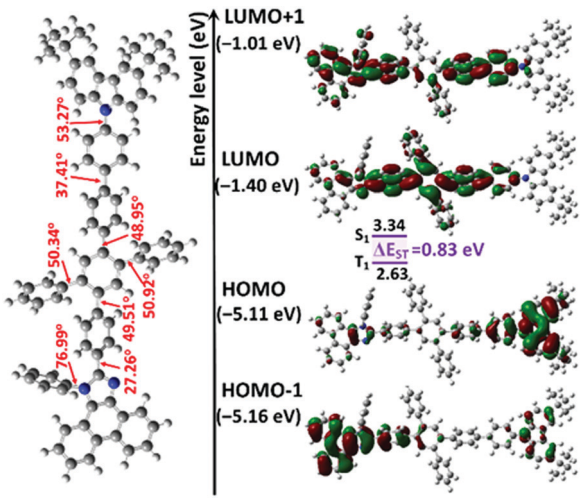

Fig. 2 The calculated optimized structures and HOMO/LUMO distributions of **PTPC**.

Photophysical properties

UV-visible absorption and PL spectra of **PTPC** were obtained to investigate its photophysical properties. As displayed in Fig. 3a and b, the absorption band around 260 and 294 nm can be considered as the π–π* transition of 1,2,4,5-TPB and carbazole. And the absorption band at 305–355 nm can be assigned to the

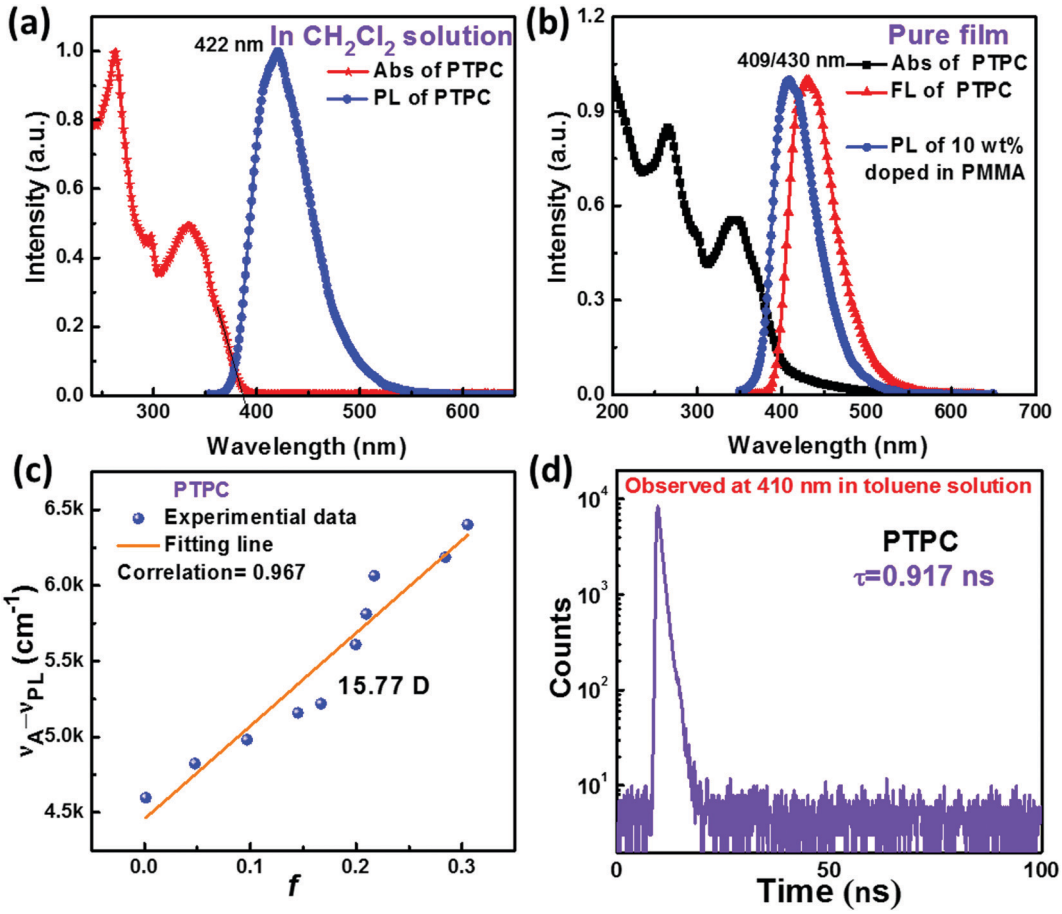

Fig. 3 (a) UV-Vis absorption and PL spectra of PTPC in CH_2Cl_2 solution (10 μM). (b) UV-Vis absorption and PL spectra of PTPC in neat films and the PL spectrum of 10 wt% PTPC doped into PMMA. (c) Solvatochromic Lippert–Mataga models of PTPC with the Stokes shift (ν_a–ν_f) *versus* orientational polarizability (*f*). (d) Transient PL decay curve in toluene solution at an excitation of 280 nm.

π–π* transition of the large and rigid molecular skeleton. The emission maxima of **PTPC** are at 422 nm in dilute CH_2Cl_2 solution (10 μM), while the emission in the neat vacuum-evaporation film (with 40 mm thickness) shows a slight red-shift with the peak at 430 nm due to the weak intermolecular interaction. In comparison, the PL spectrum of the doped film with 10 wt% **PTPC** in polymethylmethacrylate (PMMA) exhibits an obvious blue-shift with a peak at 409 nm. From the onset of UV-vis absorption in CH_2Cl_2 solution, the value of E_g was deduced to be 3.20 eV. Interestingly, PTPC exhibits the AEE feature confirmed by their PL spectra in THF/water mixtures with different water fractions (f_w) (Fig. S4, ESI†), When the $f_w \leq 60\%$, the reduction and red-shift of the PL spectra should be due to the increase of the solvent polarity of the THF/water mixture, which leads to the twisted intramolecular charge transfer process that quenches the emission. When the $f_w \geq 70\%$, owing to the worsened solvating ability of mixtures, the formation of aggregates can effectively activate the process of restriction of intramolecular motion, resulting in increased PL intensity. The reduction of PL intensity in the mixtures with $f_w \geq 90\%$ is probably caused by the formation of less emissive aggregates *via* random packing of molecules. Such a phenomenon was reported frequently in D–A type molecules.[26–29]

To further study the properties of the excited state, UV-Visible absorption and PL spectra of **PTPC** in various solvents are recorded and are shown in Fig. S5 (ESI†). When the polarity of the solvents increases (from hexane to acetonitrile), there is no obvious change of absorption spectra, while a remarkable solvatochromic effect with the red shifts of emission peaks from 396 to 426 nm is observed in the PL spectra. According to the Lippert–Mataga solvatochromic model, the Stokes shift (ν_a–ν_f) *versus* the solvent orientational polarizability (f) characteristic was estimated to analyze the properties of the S_1 state of **PTPC**. As shown in Table S2 (ESI†) and Fig. 3c, **PTPC** shows a linear relationship between ν_a–ν_f and f with a slope of 6141 (Correlation = 0.967), corresponding to the dipole moment of S_1 of 15.77 D, demonstrating that there exists only one excited state in either low polar solvents or high polar ones. This character should be a quasi-equivalent hybridization HLCT state due to the strong interstate coupling of LE and CT (charge transfer) states,[31–34] which coincides well with theoretical calculations. This can be further proved using the transient PL decay curves in different solvents where only nanosecond-scale

single-exponential decay lifetime (τ) exists. Owing to the quasi-equivalent hybridization between LE and CT states, the emitters in both toluene solution and neat films exhibit high PLQYs of 92.1% and 82.7%. According to the emission peaks of the low temperature fluorescence and phosphorescence spectra at 77 K (Fig. S8, ESI†), the S_1 and T_1 state energies can be calculated to be 3.04 and 2.48 eV, corresponding to the energy gap (ΔE_{ST}) of 0.56 eV. These results illustrates that the TADF mechanism is almost impossible for **PTPC**. As displayed in Fig. 3d, Fig. S7b and Table S3 (ESI†), the transient PL decay curves show single-exponential decay lifetimes of 0.917 and 0.988 ns, respectively, in the toluene solution and neat films. Based on the PLQY and decay lifetimes, the radiative and the non-radiative rate (k_r and k_{nr}) of **PTPC** can be calculated from the following equations: k_r = PLQY/τ, and $k_{nr} = 1/\tau - k_r$. The k_rs of **PTPC** are calculated to be 10.04 and 8.37 $\times$ 10^8 s^{-1} in the toluene solution and neat film, which are higher than those of the most reported deep-blue emitters. The k_{nr}s are calculated to be 0.87 and 1.75 $\times$ 10^8 s^{-1}.

Electrochemical and electrical properties

The HOMO energy levels of **PTPC** were obtained *via* the cyclic voltammetry (CV) measurements in anhydrous CH_2Cl_2 solution with 0.1 M tetra-*n*-butylammonium hexafluorophosphate. As displayed in Fig. S9 (ESI†), the onset oxidation potential of **PTPC** is 0.82 V, corresponding to a HOMO level of −5.41 eV. The LUMO energy level can be calculated to be −2.21 eV from the equation of LUMO = (HOMO + E_g) eV. Meanwhile, single-carrier devices were fabricated to assess their charge carrier transporting properties. The structures of the hole-only device (HOD) and electron-only device (EOD) are indium tin oxide (ITO)/1,4,5,8,9,11-hexaazatriphenylene-hexacarbonitrile (HATCN, 20 nm)/**PTPC** (80 nm)/HATCN (20 nm)/Al (150 nm) and ITO/(1,3,5-tri(phenyl-2-benzimidazolyl)benzene) (TPBi, 10 nm)/**PTPC** (80 nm)/LiF (1 nm)/Al (150 nm), respectively. It can be seen from the current density–voltage plots that current densities of the HOD and EOD are significantly increased with the increase of applied voltages (Fig. S10, ESI†), illustrating that the material **PTPC** has relatively balanced bipolar transporting capacities. The reasonable HOMO/LUMO energy levels and bipolar transporting properties of **PTPC** can ensure effective carrier injection, transportation and recombination, which is quite important for developing high efficiency and low roll-off OLEDs.

EL performance of non-doped OLEDs

To further verify the HLCT properties and EL performance of **PTPC**, a non-doped device (**D1**) with the simple structure of ITO/HATCN (20 nm)/1,1-bis[4-[*N*,*N*-di(4-tolyl)amino]phenyl]-cyclohexane (TAPC, 50 nm)/4,4′,4″-tri(*N*-carbazolyl)triphenylamine (TCTA, 5 nm)/**PTPC** (10 nm)/TPBi (40 nm)/LiF (1 nm)/Al (150 nm) was fabricated. Here, ITO was the anode, HATCN was utilized as the hole-injection layer. TPAC served as the hole-transporting layer. TCTA was used as the exciton-blocking layer. TPBi served as electron-transporting and hole-blocking layers. LiF and Al served as the electron-injection layer and cathode, respectively. The energy level alignment of the device and chemical structure of the used organic materials are shown in Fig. S11 (ESI†). The device and EL performance of the device are shown in Fig. 4 and are summarized in Table S4 (ESI†). The device **D1** exhibits a low turn-on voltage (V_{on}) of 3.1 V, corresponding to the energy of S_1 state of **PTPC**, which illustrates the highly efficient injection, transportation and recombination of holes and electrons. The luminance of 1000 and 7118 (maximum) cd m^{-2} are obtained at applied voltages of 4.7 and 7.2 V. Significantly, the device **D1** not only realizes high forward-viewing efficiencies of 6.78% (at 54.3 cd m^{-2}), 2.66 cd A^{-1}, and 2.60 lm W^{-1} for EQE, current efficiency, and power efficiency without using light out-coupling enhancement techniques, but also shows a stable deep-blue emission with a peak at 411 nm, FWHM of 55 nm and CIE coordinates of (0.156, 0.059), which is close to the standard blue CIE color coordinates of (0.15, 0.06), defined by the International Telecommunication Union (ITU). Significantly, the EQEs still remain as high as 6.73% and 6.18% at the luminance of 100 and 1000 cd m^{-2}, exhibiting a very low efficiency roll-off. As mentioned above, the possibility of the TADF process can be ruled out due to the nanosecond-scale single-exponential decay lifetime and large ΔE_{ST}, while the good linear correlation between luminance and current density implies that the TTA process is not the main emission mechanism for the device **D1** (Fig. S11c, ESI†). As seen in Fig. S3 and S12 (ESI†), the excited states of S_1, S_2, T_7 and T_8 show HLCT transition character, which ensures the existence of the high-lying reverse intersystem crossing (hRISC) process, Furthermore, a large ΔE_{ST} of 0.711 eV and small energy differences of 0.0015 and 0.0506 eV between S_1 and T_7 as well as S_2 and T_8 can effectively enhance the hRISC rate, making more singlet excitons be generated *via* two hRISC channels. It is notable that such high efficiency achieved at high luminance is one of the highest values in non-doped OLEDs with CIE$y \leq 0.07$ (Table 1).

In addition, the non-doped devices (**D2**, **D3** and **D4**) were fabricated by increasing the thickness of the emissive layer and changing the electron-transporting layer (Fig. S13, ESI†). It can be seen from Fig. 5 and Fig. S14 (ESI†) that the devices not only emit stable deep-blue light, but also show high EQEs of 6.34%, 6.71% and 6.67% for **D2**, **D3** and **D4**, respectively. These results signify that the deep-blue emitter **PTPC** has overriding characteristics of reproducibility and performance stability. Achieving such high EL performance can be attributed to the high PLQY, appropriate HOMO/LUMO energy levels, bipolar transporting properties, and HLCT excited state.

ASE properties

As mentioned above, due to the twisted, rigid and bulky molecular backbone of **PTPC**, which leads to a large spatial overlap between the HOMO and LUMO energy levels and efficiently weakens the intermolecular π–π stacking interaction and k_{nr}, realizing excellent stability (T_d: 520 °C), a high PLQY (Film: 82.7%) and a large radiative rate from S_1 to S_0 transition (Film: 8.37 $\times$ 10^8 s^{-1}). Encouraged by these results, we further

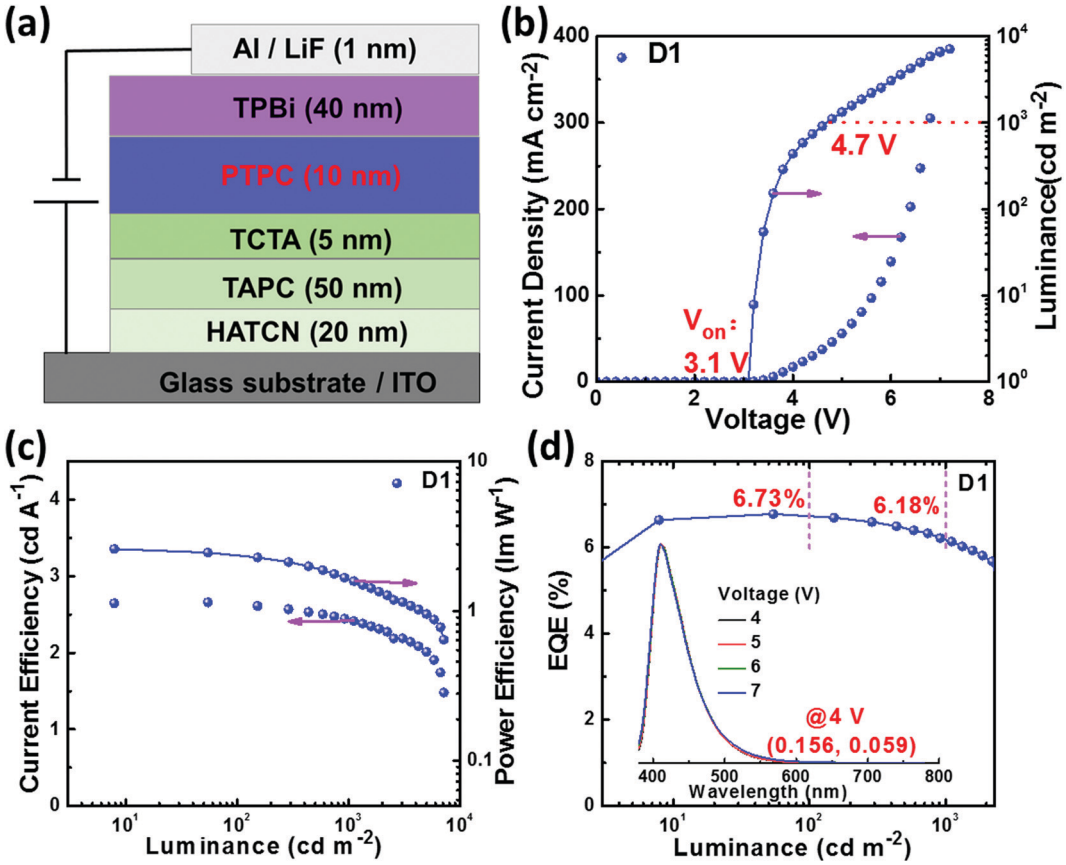

Fig. 4 The device structure diagram and EL performance of **D1**. (a) Device structure diagram. (b) Current density and luminance *versus* voltage curves. (c) Current efficiency and power efficiency *versus* luminance curves. (d) EQE *versus* luminance curves. The inset shows the normalized EL spectra at different voltages.

Table 1 The summary of reported non-doped OLEDs with CIE$y \leq 0.07$

Ref.	EQE_{max} [a] [%]	EQE_{1000} [b] [%]	CIE(x,y)
This work	6.78	6.18	(0.157, 0.059)
Ref. 1[35]	6.4	5.58	(0.151, 0.066)
Ref. 2[36]	5.08	4.44	(0.16, 0.06)
Ref. 3[37]	7.1	5.3	(0.16, 0.06)
Ref. 4[38]	6.57	—	(0.17, 0.07)
Ref. 5[39]	1.97	—	(0.16, 0.06)
Ref. 6[40]	8.9	—	(0.150, 0.060)
Ref. 7[41]	3.02	—	(0.167, 0.056)
Ref. 8[42]	3.38	—	(0.154, 0.063)
Ref. 9[43]	5.29	—	(0.155, 0.058)
Ref. 10[21]	5.74	4.8	(0.152, 0.054)
Ref. 11[44]	4.6	4.04	(0.154, 0.058)
Ref. 12[45]	3.19	—	(0.156, 0.054)
Ref. 13[46]	6.33	6.32	(0.151, 0.066)
Ref. 14[30]	4.78	—	(0.159, 0.060)
Ref. 15[47]	6.73	4.01	(0.156, 0.055)

[a] and [b] represent the maximum EQE and the value at 1000 cd m^{-2}.

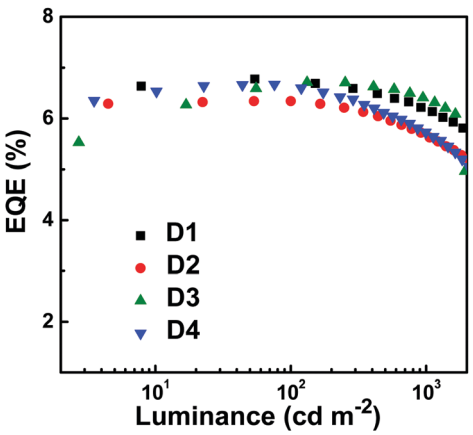

Fig. 5 EQE *versus* luminance curves of the deep-blue devices (**D1**, **D2**, **D3** and **D4**).

determined the ASE properties of **PTPC** with the hope to obtain a substantial threshold. As shown in Fig. 6a, b and Fig. S15–S19 (ESI†), with the gradual increase of excitation power, the emission of all of the studied films (2, 4, 6, 8, 10 and 100 wt%-**PTPC** blended in mCP host) exhibited spectral narrowing. The ASE effect can be well-evidenced by a clear change in the intensity slope with an increasing excitation energy density. As shown in Fig. S20a (ESI†), the ASE peaks can be adjustable from 419 to 431 nm by changing the doping concentration of **PTPC**. The optimized result was achieved by the sample with a doping concentration of 8 wt%, where the FWHM reduces from 41.0 to

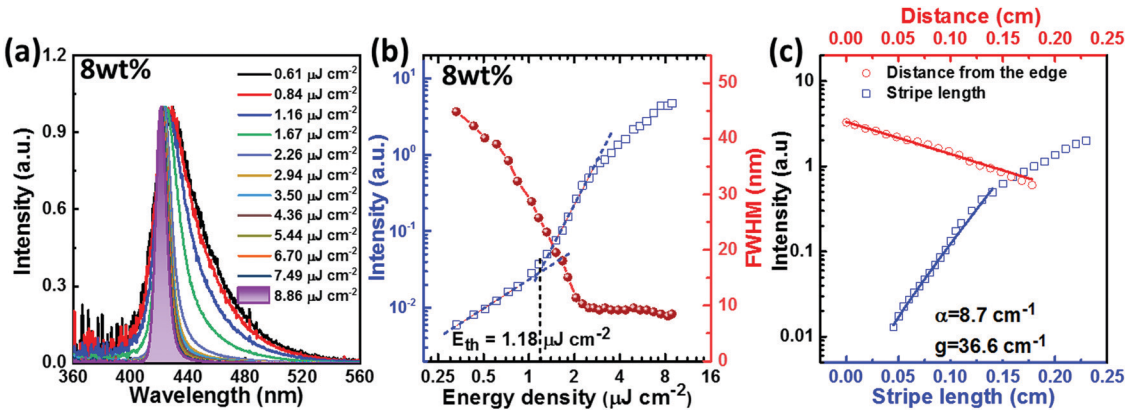

Fig. 6 (a) PL spectra of 8 wt% **PTPC** doped in mCP films at different excitation powers below and above the ASE threshold. (b) PL peak intensity and FWHM as a function of the excitation energy density of 8 wt% **PTPC** doped in mCP films. (c) Emission intensity variation with respect to both the stripe beam length and the distance from the sample edge.

8.1 nm when the excitation power was increased from 0.61 to 8.86 μJ cm^{-2}. The ASE threshold was determined to be 1.18 μJ cm^{-2} from the change in the slope of PL peak intensity *versus* excitation energy density curve (Fig. 6b), which is much lower than that of the common D–A molecules.[48–52] According to the dependence of the PL peak intensity on the stripe length, a gain coefficient (g) of 36.6 cm^{-1} can be estimated. And the loss coefficient (α) of 8.7 cm^{-1} is obtained by fitting the PL peak intensity as a function of the distance between the sample edge and the excitation region.

Most notably, the neat film not only shows a low threshold of 2.13 μJ cm^{-2}, but also exhibits more excellent photo-stability (with the 7% reduction) than the 8 wt%-**PTPC** blended mCP film (with the 82% reduction) after continuously pumping 10 000 pulses at an energy density of 8 μJ cm^{-2} (Fig. S20b, ESI†), which should be due to the stable, rigid and bulky D–π–A type molecular skeleton. These fantastic results illustrate that the HLCT emitter **PTPC** with 1,2,4,5-TPB as the π-bridge should be a promising candidate for developing highly efficient and stable deep-blue OLEDs and OSSLs. Based on this molecular system, suppressing the internal conversion process from higher triplet states (T_n) to T_1 by increasing the T_n–T_1 energy gap could be an effective avenue to further enhance the EL performance.

Conclusions

In summary, a high-performance large-size deep-blue bipolar HLCT emitter **PTPC** exhibiting AEE characteristic is successfully designed and characterized by incorporating PI and tPCz units into the 1,2,4,5-TPB core. Combining twisted and rigid molecular backbones with bulky weak D/A groups can effectively limit the π-conjugation length and suppress the aggregation quenching problem, guaranteeing good stability, a high PLQY and a fast radiative rate. Thus, it could not only achieve deep-blue light with an EL peak of 411 nm and a high EQE of 6.78% in a non-doped OLED with **PTPC** as the emitter, but also exhibit excellent ASE performance with a low threshold of 1.18 μJ cm^{-2}, which is one of the best values among those of the reported deep-blue D–A type materials. Such results provide a rational design strategy to construct efficient and stable deep-blue optoelectronic materials for future applications in OLEDs and OSSLs.

Conflicts of interest

There are no conflicts to declare.

Acknowledgements

This work was supported by grants from the National Natural Science Foundation of China (no. 52002804, 52103220, 52103017 and 22022501), the Shandong Provincial Natural Science Foundation (ZR2019ZD50) and the Open Fund of the State Key Laboratory of Luminescent Materials and Devices (2020-skllmd-12, South China University of Technology). We acknowledge Dr Zhongjie Ren at the Beijing University of Chemical Technology and Dr Shanfeng Xue at Qingdao University of Science and Technology for their help in the tests.

Notes and references

1 A. J. C. Kuehne and M. C. Gather, Organic Lasers: Recent Developments on Materials, Device Geometries, and Fabrication Techniques, *Chem. Rev.*, 2016, **116**, 12823–12864.
2 C. W. Tang and S. A. VanSlyke, Organic electroluminescent diodes, *Appl. Phys. Lett.*, 1987, **51**, 913–915.
3 X. Chen, H. Zhang, H.-J. Tan, L. Yang, P. Qin, X.-H. Zheng, S.-S. Tang, Y. Liu and Q.-X. Tong, Rational molecular design of multifunctional blue-emitting materials based on phenanthroimidazole derivatives, *Chem. – Eur. J.*, 2021, **27**, 7275–7282.
4 Y. Yin, M. U. Ali, W. Xie, H. Yang and H. Meng, Evolution of white organic light-emitting devices: from academic research to lighting and display applications, *Mater. Chem. Front.*, 2019, **3**, 970–1031.

5 B. Liu, Z.-W. Yu, D. He, M.-D. Li, W.-F. Xie and Q.-X. Tong, Productive harvesting of triplet excitons in anthracene-based emitters toward high-performance deep-blue non-doped organic light-emitting diodes, *Mater. Today Chem.*, 2022, **23**, 100630.
6 S. Chen and H. Xu, Electroluminescent materials toward near ultraviolet region, *Chem. Soc. Rev.*, 2021, **50**, 8639–8668.
7 C. W. Lee and J. Y. Lee, Above 30% External Quantum Efficiency in Blue Phosphorescent Organic Light-Emitting Diodes Using Pyrido 2,3-*b* indole Derivatives as Host Materials, *Adv. Mater.*, 2013, **25**, 5450–5454.
8 H. Shin, J.-H. Lee, C.-K. Moon, J.-S. Huh, B. Sim and J.-J. Kim, Sky-Blue Phosphorescent OLEDs with 34.1% External Quantum Efficiency Using a Low Refractive Index Electron Transporting Layer, *Adv. Mater.*, 2016, **28**, 4920–4925.
9 T. A. Lin, T. Chatterjee, W. L. Tsai, W. K. Lee, M. J. Wu, M. Jiao, K. C. Pan, C. L. Yi, C. L. Chung and K. T. Wong, Sky-Blue Organic Light Emitting Diode with 37% External Quantum Efficiency Using Thermally Activated Delayed Fluorescence from Spiroacridine-Triazine Hybrid, *Adv. Mater.*, 2016, **28**, 6976–6983.
10 J. Wei, C. Zhang, D. Zhang, Y. Zhang and L. Duan, Indolo[3,2,1-*jk*]carbazole Embedded Multiple in Esonance Fluorophors for Narrowband Deep-blue Electroluminescence with EQE ~34.7% and CIE*y* ~ 0.085, *Angew. Chem., Int. Ed.*, 2021, **60**, 12269–12273.
11 R. Braveenth, H. Lee, J. D. Park, K. J. Yang, S. J. Hwang, K. R. Naveen, R. Lampande and J. H. Kwon, Achieving Narrow FWHM and High EQE Over 38% in Blue OLEDs Using Rigid Heteroatom-Based Deep Blue TADF Sensitized Host, *Adv. Funct. Mater.*, 2021, **31**, 2105805.
12 C. Poriel and J. Rault-Berthelot, Designing Host Materials for the Emissive Layer of Single-Layer Phosphorescent Organic Light-Emitting Diodes: Toward Simplified Organic Devices, *Adv. Funct. Mater.*, 2021, **31**, 2010547.
13 T. Chatterjee and K.-T. Wong, Perspective on Host Materials for Thermally Activated Delayed Fluorescence Organic Light Emitting Diodes, *Adv. Opt. Mater.*, 2019, **7**, 1800565.
14 X. Yang, G. Zhou and W.-Y. Wong, Functionalization of phosphorescent emitters and their host materials by main-group elements for phosphorescent organic light-emitting devices, *Chem. Soc. Rev.*, 2015, **44**, 8484–8575.
15 Y. Tao, C. Yang and J. Qin, Organic host materials for phosphorescent organic light-emitting diodes, *Chem. Soc. Rev.*, 2011, **40**, 2943–2970.
16 C. Murawski, K. Leo and M. C. Gather, Efficiency Roll-Off in Organic Light-Emitting Diodes, *Adv. Mater.*, 2013, **25**, 6801–6827.
17 D. Wang, C. Cheng, T. Tsuboi and Q. Zhang, Degradation Mechanisms in Blue Organic Light-Emitting Diodes, *CCS Chem.*, 2020, **2**, 1278–1296.
18 Y. Xu, P. Xu, D. Hu and Y. Ma, Recent progress in hot exciton materials for organic light-emitting diodes, *Chem. Soc. Rev.*, 2021, **50**, 1030–1069.
19 G.-X. Yang, H.-J. Tan, J.-W. Zhao, J.-J. Zhu, X. He, J.-X. Jian, M.-H. Zhou, S.-L. Tao and Q.-X. Tong, Structurally modified [1,2,4]triazolo[1,5-*a*]pyridine derivatives as promising materials for highly efficient blue fluorescent organic light-emitting diodes, *Chem. Eng. J.*, 2022, **445**, 136813.
20 W. Liu, S. Ying, R. Guo, X. Qiao, P. Leng, Q. Zhang, Y. Wang, D. Ma and L. Wang, Nondoped blue fluorescent organic light-emitting diodes based on benzonitrile-anthracene derivative with 10.06% external quantum efficiency and low efficiency roll-off, *J. Mater. Chem. C*, 2019, **7**, 1014–1021.
21 X. Qiu, S. Ying, C. Wang, M. Hanif, Y. Xu, Y. Li, R. Zhao, D. Hu, D. Ma and Y. Ma, Novel 9,9-dimethylfluorene-bridged D–π–A-type fluorophores with a hybridized local and charge-transfer excited state for deep-blue electroluminescence with CIE*y* ~ 0.05, *J. Mater. Chem. C*, 2019, **7**, 592–600.
22 R. Guo, W. Liu, S. Ying, Y. Xu, Y. Wen, Y. Wang, D. Hu, X. Qiao, B. Yang, D. Ma and L. Wang, Exceptionally efficient deep blue anthracene-based luminogens: design, synthesis, photophysical, and electroluminescent mechanisms, *Sci. Bull.*, 2021, **66**, 2090–2098.
23 Y. Im, S. Y. Byun, J. H. Kim, D. R. Lee, C. S. Oh, K. S. Yook and J. Y. Lee, Recent Progress in High-Efficiency Blue-Light-Emitting Materials for Organic Light-Emitting Diodes, *Adv. Funct. Mater.*, 2017, **27**, 1603007.
24 B. Zhong, S. Wang, Y. Xiao and X. Li, Bipolar Blue Fluorescent Materials for Organic Light-Emitting Devices, *Prog. Chem.*, 2015, **27**, 986–1001.
25 S.-J. Zou, Y. Shen, F.-M. Xie, J.-D. Chen, Y.-Q. Li and J.-X. Tang, Recent advances in organic light-emitting diodes: toward smart lighting and displays, *Mater. Chem. Front.*, 2020, **4**, 788–820.
26 L. Li, M. Chen, H. Zhang, H. Nie, J. Z. Sun, A. Qin and B. Z. Tang, Influence of the number and substitution position of phenyl groups on the aggregation-enhanced emission of benzene-cored luminogens, *Chem. Commun.*, 2015, **51**, 4830–4833.
27 X. M. Guo, P. S. Yuan, J. Z. Fan, X. F. Qiao, D. Z. Yang, Y. F. Dai, Q. Sun, A. J. Qin, B. Z. Tang and D. G. Ma, Unraveling the Important Role of High-Lying Triplet-Lowest Excited Singlet Transitions in Achieving Highly Efficient Deep-Blue AIE-Based OLEDs, *Adv. Mater.*, 2021, **33**, 2006953.
28 M. Shimizu and T. Sakurai, Organic fluorophores that emit ultraviolet light in the aggregated state, *Aggregate*, 2022, **3**, e144.
29 Z. Xu, J. Gu, X. Qiao, A. Qin, B. Z. Tang and D. Ma, Highly Efficient Deep Blue Aggregation-Induced Emission Organic Molecule: A Promising Multifunctional Electroluminescence Material for Blue/Green/Orange/Red/White OLEDs with Superior Efficiency and Low Roll-Off, *ACS Photonics*, 2019, **6**, 767–778.
30 P. Han, C. Lin, D. Ma, A. Qin and B. Z. Tang, Violet-Blue Emitters Featuring Aggregation-Enhanced Emission Characteristics for Nondoped OLEDs with CIE*y* Smaller than 0.046, *ACS Appl. Mater. Interfaces*, 2020, **12**, 46366–46372.
31 S. Zhang, L. Yao, Q. Peng, W. Li, Y. Pan, R. Xiao, Y. Gao, C. Gu, Z. Wang, P. Lu, F. Li, S. Su, B. Yang and Y. Ma, Achieving a Significantly Increased Efficiency in Nondoped

Pure Blue Fluorescent OLED: A Quasi-Equivalent Hybridized Excited State, *Adv. Funct. Mater.*, 2015, **25**, 1755–1762.

32 H. Zhang, B. Zhang, Y. Zhang, Z. Xu, H. Wu, P. A. Yin, Z. Wang, Z. Zhao, D. Ma and B. Z. Tang, A Multifunctional Blue-Emitting Material Designed via Tuning Distribution of Hybridized Excited-State for High-Performance Blue and Host-Sensitized OLEDs, *Adv. Funct. Mater.*, 2020, **30**, 2002323.

33 S. B. Xiao, S. T. Zhang, Y. Gao, X. Q. Yang, H. C. Liu, W. J. Li and B. Yang, Efficient and stable deep-blue narrow-spectrum electroluminescence based on hybridized local and charge-transfer (HLCT) state, *Dyes Pigm.*, 2021, **193**, 109482.

34 Y. Liu, X. Man, Q. Bai, H. Liu, P. Liu, Y. Fu, D. Hu, P. Lu and Y. Ma, Highly Efficient Blue Organic Light-Emitting Diode Based on a Pyrene[4,5-*d*]Imidazole-Pyrene Molecule, *CCS Chem.*, 2021, **3**, 545–558.

35 S. Ye, Y. Wang, R. Guo, Q. Zhang, X. Lv, Y. Duan, P. Leng, S. Sun and L. Wang, Asymmetric anthracene derivatives as multifunctional electronic materials for constructing simplified and efficient non-doped homogeneous deep blue fluorescent OLEDs, *Chem. Eng. J.*, 2020, **393**, 124694.

36 Z.-L. Zhu, S.-F. Ni, W.-C. Chen, M. Chen, J.-J. Zhu, Y. Yuan, Q.-X. Tong, F.-L. Wong and C.-S. Lee, Tuning electrical properties of phenanthroimidazole derivatives to construct multifunctional deep-blue electroluminescent materials, *J. Mater. Chem. C*, 2018, **6**, 3584–3592.

37 Y. Zheng, X. Zhu, Z. Ni, X. Wang, Z. Zhong, X. J. Feng, Z. Zhao and H. Lu, Bipolar Molecules with Hybridized Local and Charge-Transfer State for Highly Efficient Deep-Blue Organic Light-Emitting Diodes with EQE of 7.4% and CIEy $\sim$ 0.05, *Adv. Opt. Mater.*, 2021, **9**, 2100965.

38 S. Xue, X. Qiu, S. Ying, Y. Lu, Y. Pan, Q. Sun, C. Gu and W. Yang, Highly Efficient Nondoped Near-Ultraviolet Electroluminescence with an External Quantum Efficiency Greater Than 6.5% Based on a Carbazole-Triazole Hybrid Molecule with High and Balanced Charge Mobility, *Adv. Opt. Mater.*, 2017, **5**, 1700747.

39 S. Jhulki, A. K. Mishra, A. Ghosh, T. J. Chow and J. N. Moorthy, Deep blue-emissive bifunctional (hole-transporting + emissive) materials with CIEy $\sim$ 0.06 based on a 'U'-shaped phenanthrene scaffold for application in organic light-emitting diodes, *J. Mater. Chem. C*, 2016, **4**, 9310–9315.

40 J.-S. Huh, Y. H. Ha, S.-K. Kwon, Y.-H. Kim and J.-J. Kim, Design Strategy of Anthracene-Based Fluorophores toward High-Efficiency Deep Blue Organic Light-Emitting Diodes Utilizing Triplet–Triplet Fusion, *ACS Appl. Mater. Interfaces*, 2020, **12**, 15422–15429.

41 Z. Gao, Z. Wang, T. Shan, Y. Liu, F. Shen, Y. Pan, H. Zhang, X. He, P. Lu, B. Yang and Y. Ma, High-efficiency deep blue fluorescent emitters based on phenanthro[9,10-*d*]imidazole substituted carbazole and their applications in organic light emitting diodes, *Org. Electron.*, 2014, **15**, 2667–2676.

42 W.-C. Chen, Y. Yuan, S.-F. Ni, Q.-X. Tong, F.-L. Wong and C.-S. Lee, Achieving efficient violet-blue electroluminescence with CIEy $<$ 0.06 and EQE $>$ 6% from naphthyl-linked phenanthroimidazole–carbazole hybrid fluorophores, *Chem. Sci.*, 2017, **8**, 3599–3608.

43 Z.-Y. Wang, J.-W. Zhao, B. Liu, C. Cao, P. Li, Q.-X. Tong and S.-L. Tao, Universal materials for high performance violet-blue OLEDs (CIEy $<$ 0.06) and PhOLEDs, *Dyes Pigm.*, 2019, **163**, 213–220.

44 J. Zhao, B. Liu, Z. Wang, Q. Tong, X. Du, C. Zheng, H. Lin, S. Tao and X. Zhang, EQE Climbing Over 6% at High Brightness of 14 350 cd m^{-2} in Deep-Blue OLEDs Based on Hybridized Local and Charge-Transfer Fluorescence, *ACS Appl. Mater. Interfaces*, 2018, **10**, 9629–9637.

45 H. Zhou, M. Yin, Z. Zhao, Y. Miao, X. Jin, J. Huang, Z. Gao, H. Wang, J. Su and H. Tian, Novel carbazole-based multifunctional materials with a hybridized local and charge-transfer excited state acting as deep-blue emitters and phosphorescent hosts for highly efficient organic light-emitting diodes, *J. Mater. Chem. C*, 2021, **9**, 5899–5907.

46 B. Liu, Z.-W. Yu, D. He, Z.-L. Zhu, J. Zheng, Y.-D. Yu, W.-F. Xie, Q.-X. Tong and C.-S. Lee, Ambipolar D–A type bifunctional materials with hybridized local and charge-transfer excited state for high performance electroluminescence with EQE of 7.20% and CIEy $\sim$ 0.06, *J. Mater. Chem. C*, 2017, **5**, 5402–5410.

47 Z. Li, N. Xie, Y. Xu, C. Li, X. Mu and Y. Wang, Fluorine-Substituted Phenanthro[9,10-d]imidazole Derivatives with Optimized Charge-Transfer Characteristics for Efficient Deep-Blue Emitters, *Org. Mater.*, 2020, **02**, 011–019.

48 A. Khan, X. Tang, C. Zhong, Q. Wang, S. Y. Yang, F. C. Kong, S. Yuan, A. S. D. Sandanayaka, C. Adachi, Z. Q. Jiang and L. S. Liao, Intramolecular-Locked High Efficiency Ultrapure Violet-Blue (CIE-y $<$0.046) Thermally Activated Delayed Fluorescence Emitters Exhibiting Amplified Spontaneous Emission, *Adv. Funct. Mater.*, 2021, **31**, 2009488.

49 U. Balijapalli, X. Tang, D. Okada, Y. T. Lee, B. S. B. Karunathilaka, M. Auffray, G. Tumen-Ulzii, Y. Tsuchiya, A. S. D. Sandanayaka, T. Matsushima, H. Nakanotani and C. Adachi, 2,6-Dicarbonitrile Diphenyl-1λ^5-Phosphinine (DCNP)—A Robust Conjugated Building Block for Multi-Functional Dyes Exhibiting Tunable Amplified Spontaneous Emission, *Adv. Opt. Mater.*, 2021, **9**, 2101122.

50 X. Tang, U. Balijapalli, D. Okada, B. S. B. Karunathilaka, C. A. M. Senevirathne, Y. T. Lee, Z. Feng, A. S. D. Sandanayaka, T. Matsushima and C. Adachi, Electron-Affinity Substituent in 2,6-Dicarbonitrile Diphenyl-1λ^5-Phosphinine Towards High-Quality Organic Lasing and Electroluminescence under High Current Injection, *Adv. Funct. Mater.*, 2021, **31**, 2104529.

51 A. Shukla, N. R. Wallwork, X. Li, J. Sobus, V. T. N. Mai, S. K. M. McGregor, K. Chen, R. J. Lepage, E. H. Krenske, E. G. Moore, E. B. Namdas and S. C. Lo, Deep-Red Lasing and Amplified Spontaneous Emission from Nature Inspired Bay-Annulated Indigo Derivatives, *Adv. Opt. Mater.*, 2019, **8**, 1901350.

52 X. Tang, Y.-T. Lee, Z. Feng, S. Y. Ko, J. W. Wu, V. Placide, J.-C. Ribierre, A. D'Aléo and C. Adachi, Color-Tunable Low-Threshold Amplified Spontaneous Emission from Yellow to Near-Infrared (NIR) Based on Donor–Spacer–Acceptor–Spacer–Donor Linear Dyes, *ACS Mater. Lett.*, 2020, **2**, 1567–1574.